EPJ B
Condensed Matter and Complex Systems
EPJ.org
your physics journal

Eur. Phys. J. B (2018) 91: 169 DOI: 10.1140/epjb/e2018-90170-1

An efficient implementation of two-component relativistic density functional theory with torque-free auxiliary variables

Alessio Petrone, David B. Williams-Young, Shichao Sun, Torin F. Stetina, and Xiaosong Li

edp sciences
Società Italiana di Fisica
Springer

Eur. Phys. J. B (2018) 91: 169
https://doi.org/10.1140/epjb/e2018-90170-1

THE EUROPEAN PHYSICAL JOURNAL B

Regular Article

An efficient implementation of two-component relativistic density functional theory with torque-free auxiliary variables*

Alessio Petrone[a], David B. Williams-Young[a], Shichao Sun, Torin F. Stetina, and Xiaosong Li[b]

Department of Chemistry, University of Washington, Seattle, WA 98195, USA

Received 13 March 2018 / Received in final form 17 May 2018
Published online 23 July 2018

Abstract. An integration and assembly strategy for efficient evaluation of the exchange correlation term in relativistic density functional theory within two-component Kohn–Sham framework is presented. Working equations that both take into account all the components of the spin magnetization and can exploit parallelism, optimized cache utilization, and micro-architecture specific-floating point operations are discussed in detail in this work. The presented assembly of the exchange correlation potential, suitable for both open and closed shell systems, uses spinor density and a set of auxiliary variables, ensuring easy retrofitting of existing density functionals designed for collinear density. The used auxiliary variables in this paper, based on the scalar and non-collinear density, can preserve non-zero exchange correlation magnetic field local torque, without violating the required overall zero torque, even for GGA functionals. This is mandatory to obtain accurate spin dynamics and proper time evolution of the magnetization. Spin frustrated hydrogen rings are used to validate the current implementation and phenoxy radicals of different sizes are used to monitor the performance. This approach is a step towards extending the applicability of relativistic two-component DFT to systems of large size (>100 atoms).

1 Introduction

Density functional theory (DFT) [1,2] and time-dependent density functional theory (TDDFT) [3–7] have become the primary investigative tool for quantum chemical calculations regarding systems at large, experimentally relevant scales. The primary reasons for their successes are the excellent balance of accuracy and computational cost, and the vast availability through the development of efficient and reliable DFT software capable of leveraging the latest advances in high–performance computing [8]. DFT presents an attractive alternative to wave function based correlation methods which depend on computationally expensive many-body expansions, such as multi-configurational self-consistent-field and coupled-cluster theory [9–11], because it is able to account for many-body correlation effects through an effective one-body operator known as the exchange correlation (xc) potential. Efficient and robust numerical integration techniques for the xc potential have been thoroughly studied throughout the years [12–18], and their proper application is crucial to the practicality and applicability of DFT methods. The wide adoption of DFT/TDDFT in the scientific community as a whole has enabled routine, ab initio characterization of both ground and excited state properties for large macromolecular systems such as those of biological [19–21] and materials [22–27] interest and their transient behavior [28–31].

Recently, there has been a resurgence of interest in the materials community for the development and design of materials which exploit properties of electronic spin in their applications, such as magnetic materials, spintronic devices, and catalytic active sites [32–35]. As such, there is a strong need for electronic structure theories that are capable of treating electronic spins in large scale systems. Thus, motivated by its success in other aspects of materials research, there has been a large emphasis in recent years on the extension of existing DFT/TDDFT methods to properly include electronic spin and spin interactions.

At its core, a rigorous treatment of electronic spin and its interaction with materials in quantum systems must be rooted in relativistic quantum mechanics [36–39]. Although typically thought to be of consequence only in heavy-elements, the introduction of spin-couplings into the Hamiltonian has been demonstrated to yield profound effects even in light elements [38], which may be physically realized in systems such as doped nanodiamonds which have recently been recognized as fantastic candidates for the next generation of spintronic devices and q-bits in quantum computers [24,40–44]. Due to

* Contribution to the Topical Issue "Special issue in honor of Hardy Gross", edited by C.A. Ullrich, F.M.S. Nogueira, A. Rubio, and M.A.L. Marques.

[a] AP and DBW contributed equally.

[b] e-mail: xsli@uw.edu

this centralized importance in the treatment of electronic spin, there has been a lot of effort in recent years to extend existing electronic structure methods to include relativistic effects, chief among them being extensions of DFT/TDDFT based methods in both the ground [45–48] and excited [49–53] electronic states. A rigorous relativistic description of a quantum system, based on the Dirac–Coulomb–Hamiltonian [37,39,50,51,54], explicitly treats both the electronic and positronic nature of the electronic wave function through a Dirac bispinor (four-component) wave functions. Further, in the context of DFT, relativistic analogues to the Hohenberg–Kohn theorems require the exact energy functional not only to be a functional of the electronic density, but also of the current density [37,39,55–62]. While some work has gone into the development of these types of functionals [63–69], the bulk of widely used exchange correlation functionals do not include these effects due to the fact that their contribution is typically small.

The positronic nature of the electronic wave function, arising from its relativistic treatment, is of great consequence in the study of chemical systems as it gives rise to many important phenomena such a spin–orbit coupling, the inert pair effect, spin-forbidden reactivity [38,70–73]. However, despite its importance, its explicit treatment is often not needed for a qualitatively correct description of its consequences in molecular systems. It is often advantageous from a practical, as well as aesthetic perspective, to transform the four-component Dirac–Coulomb–Hamiltonian to a two-component (spinor) form which closely resembles non-relativistic electronic structure theories [74–77]. In essence, two-component relativistic methods aim to fold the positronic component of the four-component wave function into the electronic component to form a pseudo relativistic spinor wave function. As such, it will be two-component relativistic methods that will be treated in this work.

One of the central challenges in relativistic DFT is in that the introduction of spin couplings into the Hamiltonian necessarily introduce spin non-collinearity in the electronic density for open-shell systems, i.e the spin magnetization vector is no longer restricted to coincide with the z-axis [37,39,78]. In this regard, unlike the collinear theory, non-collinear DFT requires the functional to depend on charge density and spin magnetization vector. Unfortunately, density functionals commonly employed in quantum chemistry have been developed for collinear densities, and therefore, there is no straightforward way to employ them in non-collinear systems. Several efforts have been made to adapt common density functionals developed for collinear densities to the general case to be used in relativistic calculations, both in the context of relativistic two-component [46,53,79–84] and four-component [45,46,85–87] methods. In this context, any non-collinear DFT generalization needs also to pay particular attention on preserving the property that the self-consistent xc magnetic field cannot exert a net torque on the system as a whole (zero-torque theorem) [88]. On the other hand, the local torque does not need to vanish identically at every point in space, since this local contribution is required to obtain accurate spin dynamics and a proper time-evolution of the magnetization [53,82–84,88–90]. However, in stark contrast to its non-relativistic collinear counterpart, no work has gone into developing highly optimized numerical integration techniques for these relativistic DFT methods. Thus, in this work, we outline an efficient algorithm and practical considerations for the integration of the xc potential in non-collinear relativistic DFT.

2 Two-component Kohn–Sham density functional theory

In this section we provide a brief overview of approximate relativistic electronic Hamiltonians and their two-component counterparts in the context of Kohn–Sham density functional theory. We refer the reader to standard texts on the subject [37,39] for a more thorough treatment. Neglecting coupling to external fields and retardation effects, and within the Born–Oppenheimer approximation, relativistic many-body quantum mechanics is approximately governed by the Dirac–Coulomb (DC) Hamiltonian,

$$\hat{H}^{DC} = \sum_{i}^{N} \left(\hat{h}^{D}(i) + \hat{V}(i) \right) + \sum_{i<j}^{N} \hat{g}^{C}(i,j), \tag{1}$$

where the sums over i and j are sums over the N electrons in the quantum system. Here, $\hat{h}^{D}(i)$ is the single body free–particle Dirac (D) operator and is given in atomic units by,

$$\hat{h}^{D}(i) = \begin{bmatrix} 0 & 0 \\ 0 & -2c^2 \end{bmatrix} \otimes \boldsymbol{I}_2 + c \sum_{k} \begin{bmatrix} 0 & \hat{p}_k(i) \\ \hat{p}_k(i) & 0 \end{bmatrix} \otimes \boldsymbol{\sigma}_k, \tag{2}$$

where $\hat{\boldsymbol{p}}(i)$ is the momentum operator for the ith particle, $\boldsymbol{I}_2$ is the 2-by-2 identity matrix, and $\{\boldsymbol{\sigma}_k\}$ is the set of Pauli matrices.

$$\boldsymbol{I}_2 = \begin{pmatrix} 1 & 0 \\ 0 & 1 \end{pmatrix}, \quad \boldsymbol{\sigma}_z = \begin{pmatrix} 1 & 0 \\ 0 & -1 \end{pmatrix}, \quad \boldsymbol{\sigma}_y = \begin{pmatrix} 0 & -i \\ i & 0 \end{pmatrix}, \quad \boldsymbol{\sigma}_x = \begin{pmatrix} 0 & 1 \\ 1 & 0 \end{pmatrix}. \tag{3}$$

$\hat{V}(i)$ is the one-body external potential, which in the context of this work will be solely described by the electron–nuclear Coulomb interaction,

$$\hat{V}(i) = -\left(\sum_{A} \int_{\mathbb{R}^3} \mathrm{d}^3\mathbf{R} \, \frac{P_A(\mathbf{R})}{|\mathbf{R} - \mathbf{r}_i|} \right) \otimes \boldsymbol{I}_4, \tag{4}$$

where P_A is the nuclear charge density of the A-th nucleus, and will be taken to be Gaussian in character [91]. $\hat{g}^{C}(i,j)$ is the two-body Coulomb interaction between electrons,

given by

$$\hat{g}^C(i,j) = \left(\frac{1}{|\mathbf{r}_i - \mathbf{r}_j|}\right) \otimes \boldsymbol{I}_4. \tag{5}$$

From the definitions given by equations (2)–(5), it is clear that $\hat{H}^{DC}$ acts on a 4-component wave function, Ψ, such that

$$i\partial_t \Psi = \hat{H}^{DC}\Psi, \quad \Psi \in \mathbb{C}^4. \tag{6}$$

For subsequent developments, it will be useful to separate Ψ into its electronic (Ψ^L) and positronic (Ψ^S) components

$$\Psi = \begin{pmatrix} \Psi^L \\ \Psi^S \end{pmatrix}, \tag{7}$$

and further into their spin components,

$$\Psi^X = \begin{pmatrix} \Psi^X_\alpha \\ \Psi^X_\beta \end{pmatrix}, \quad X \in \{L, S\}. \tag{8}$$

From equations (7) and (8) we may define the electronic density, ρ,

$$\rho = \Psi\Psi^\dagger = \begin{bmatrix} \rho^{LL}_{\alpha\alpha} & \rho^{LL}_{\alpha\beta} & \rho^{LS}_{\alpha\alpha} & \rho^{LS}_{\alpha\beta} \\ \rho^{LL}_{\beta\alpha} & \rho^{LL}_{\beta\beta} & \rho^{LS}_{\beta\alpha} & \rho^{LS}_{\beta\beta} \\ \rho^{SL}_{\alpha\alpha} & \rho^{SL}_{\alpha\beta} & \rho^{SS}_{\alpha\alpha} & \rho^{SS}_{\alpha\beta} \\ \rho^{SL}_{\beta\alpha} & \rho^{SL}_{\beta\beta} & \rho^{SS}_{\beta\alpha} & \rho^{SS}_{\beta\beta} \end{bmatrix}, \tag{9}$$

where we have separated ρ into its binary components which are given by

$$\rho^{XY}_{\sigma\sigma'}(\mathbf{r}) = N \int \mathrm{d}^3\mathbf{r}_2 \cdots \int \mathrm{d}^3\mathbf{r}_N \times \Psi^{X*}_\sigma(\mathbf{r}, \mathbf{r}_2, \ldots, \mathbf{r}_N)\Psi^Y_{\sigma'}(\mathbf{r}, \mathbf{r}_2, \ldots, \mathbf{r}_N). \tag{10}$$

Formally, Kohn–Sham density functional theory may be extended to such a four-component description of the electronic density in terms of the energy functional [45],

$$E[\rho] = T_s[\rho] + V[\rho] + J[\rho] + E_{\mathrm{xc}}[\rho] + V_{\mathrm{nn}}. \tag{11}$$

With the exception of T_s, the functionals adopt a similar form to those of non-relativistic Kohn–Sham,

$$V[\rho] = \int \mathrm{d}^3\mathbf{r}\ \mathrm{Tr}[\hat{V}(\mathbf{r})\rho(\mathbf{r})], \tag{12}$$

$$J[\rho] = \int \mathrm{d}^3\mathbf{r} \int \mathrm{d}^3\mathbf{r}'\ \mathrm{Tr}[\hat{g}^C(\mathbf{r}, \mathbf{r}')\rho(\mathbf{r})\rho(\mathbf{r}')], \tag{13}$$

$$V_{\mathrm{nn}} = \sum_{A<B} \int \mathrm{d}^3\mathbf{R} \int \mathrm{d}^3\mathbf{R}' \frac{P_A(\mathbf{R})P_B(\mathbf{R}')}{|\mathbf{R} - \mathbf{R}'|}. \tag{14}$$

Unlike non-relativistic Kohn–Sham theory, where T_s is written as the expectation value of the kinetic energy operator in the non-interacting ground state Slater determinant through the introduction of single-particle orbitals, in four-component theory, T_s is given by the expectation value of the free particle Dirac operator,

$$T_s[\rho] = \sum_i \int \mathrm{d}^3\mathbf{r}\ \psi^\dagger_i(\mathbf{r})\hat{h^D}(i)\psi_i(\mathbf{r}). \tag{15}$$

Here $\{\psi_i \in \mathbb{C}^4\}$ is a set of orbitals which exhibit the same block form as equations (7) and (8), the single particle basis for the ground state Slater determinant. The operative term in equation (11) is the exchange correlation energy functional, E_{xc}, which accounts for the quantum many-body effects in Kohn–Sham theory. As the exact E_{xc} is unknown, the proper choice of its approximation is paramount in practical Kohn–Sham calculations. In this work, we will limit our discussion to those functionals which may be characterized under the hybrid generalized gradient approximation (hybrid GGA), where E_{xc} takes the form

$$E_{\mathrm{xc}}[\rho] = E^{GGA}_{\mathrm{xc}}[\rho, \nabla\rho] + c_x E^{HF}_x[\rho]. \tag{16}$$

Here, the full E_{xc} has been partitioned into a pure GGA exchange correlation functional, E^{GGA}_{xc}, which is a functional of the electronic density and its gradient, and a scaled ($c_x \in [0, 1]$) Hartree–Fock exchange contribution, E^{HF}_x.

Minimizing equation (11) with respect to $\{\psi_i\}$, we may formulate the Kohn–Sham eigenproblem,

$$\hat{f}^{DKS}(\mathbf{r})\psi_i(\mathbf{r}) = \epsilon_i\psi_i(\mathbf{r}), \tag{17}$$

where $\{\epsilon_i\}$ is the set of canonical Kohn–Sham orbital eigenenergies and,

$$\hat{f}^{DKS}(\mathbf{r}) = \hat{h}^D(\mathbf{r}) + \hat{V}(\mathbf{r}) + \hat{J}(\mathbf{r}) + \hat{V}^{xc}(\mathbf{r}), \tag{18}$$

$\hat{J}$ is the effective Coulomb operator,

$$\hat{J}(\mathbf{r}) = \int \mathrm{d}^3\mathbf{r}'\ \frac{\rho(\mathbf{r}')}{|\mathbf{r} - \mathbf{r}'|}, \tag{19}$$

and $\hat{V}^{xc}$ is the exchange correlation potential,

$$\hat{V}^{xc}(\mathbf{r}) = \frac{\delta E_{\mathrm{xc}}}{\delta\rho(\mathbf{r})}. \tag{20}$$

As functional derivatives are covariant under change of basis, the structure of $\hat{V}^{xc}$ in equation (20) formally has the same block structure as equation (9).

Of interest in this work, two-component relativistic Hamiltonians are obtained, in general, through a similarity transformation under a unitary operator, $\hat{\mathcal{U}}$, which effectively folds the positronic component of the electronic wave function into a spinor form which block diagonalizes equation (17),

$$\hat{f}^{DKS}(\mathbf{r}) \mapsto \hat{f}^{2C}(\mathbf{r}) = \hat{\mathcal{U}}^\dagger \hat{f}^{DKS}(\mathbf{r})\hat{\mathcal{U}} = \begin{bmatrix} \hat{f}^+(\mathbf{r}) & 0 \\ 0 & \hat{f}^-(\mathbf{r}) \end{bmatrix}, \tag{21}$$

$$\psi_i(\mathbf{r}) \mapsto \hat{\mathcal{U}}^\dagger \psi_i(\mathbf{r}) = \begin{bmatrix} \phi_i(\mathbf{r}) \\ 0 \end{bmatrix}. \tag{22}$$

Thus, equation (17) is reduced to

$$\hat{f}^+(\mathbf{r})\phi_i(\mathbf{r}) = \epsilon_i \phi_i(\mathbf{r}), \tag{23}$$

where $\{\phi_i\}$ are the effective two-component orbitals which contain information regarding to both the electronic and positronic components of the relativistic wave function. It is useful to note that ϕ_i exhibits the same block form as equation (8) and is formally referred to as a spinor. Equation (22) implies that the electronic density may now be written, effectively, in two-component form,

$$\rho(\mathbf{r}) = \sum_i \psi_i(\mathbf{r})\psi_i^\dagger(\mathbf{r}) = \begin{bmatrix} \rho_{\alpha\alpha}(\mathbf{r}) & \rho_{\alpha\beta}(\mathbf{r}) & 0 & 0 \\ \rho_{\beta\alpha}(\mathbf{r}) & \rho_{\beta\beta}(\mathbf{r}) & 0 & 0 \\ 0 & 0 & 0 & 0 \\ 0 & 0 & 0 & 0 \end{bmatrix}, \tag{24}$$

where

$$\rho_{\sigma\sigma'}(\mathbf{r}) = \sum_i \phi_i^\sigma(\mathbf{r}) \phi_i^{\sigma'\dagger}(\mathbf{r}). \tag{25}$$

Formally, the expressions given in equations (21) and (22) are exact given an exact $\hat{\mathcal{U}}$. However, such an exact expression for $\hat{\mathcal{U}}$ is not possible, in general, for many-body Hamiltonians [92], thus one must utilize approximate transformations. There exist many approximate two-component methods in the literature [39,74,75,92–95]. In this work, we will focus on the exact two-component (X2C) method [47,77,96–99], which is formally exact for a single electron system. We refer the reader elsewhere for practical considerations regarding the implementation of the X2C method [98].

Within the linear combination of atomic orbitals (LCAO) description of the molecular orbitals in a real atomic basis $\{\chi_\mu\}$,

$$\phi_i^\sigma(\mathbf{r}) = \sum_\mu C_{\mu i}^\sigma \chi_\mu(\mathbf{r}). \tag{26}$$

Equation (23) may be cast into matrix form,

$$\mathbf{F}[\mathbf{P}]\mathbf{C} = \mathbf{S}\mathbf{C}\boldsymbol{\epsilon}, \tag{27}$$

where $\mathbf{F}$ is the Kohn–Sham Fock matrix depends on $\mathbf{P}$, the one-particle density matrix. $\mathbf{C}$ is the matrix of molecular orbital coefficients, $\mathbf{S}$ is the overlap matrix, and $\boldsymbol{\epsilon}$ is the diagonal matrix of canonical Kohn–Sham orbital eigenenergies. Due to the spinor structure of $\{\phi_i\}$, $\mathbf{F}$ and $\mathbf{P}$ formally have the spin-blocked structure

$$\mathbf{X} = \begin{bmatrix} \mathbf{X}^{\alpha\alpha} & \mathbf{X}^{\alpha\beta} \\ \mathbf{X}^{\beta\alpha} & \mathbf{X}^{\beta\beta} \end{bmatrix}, \quad \mathbf{X} \in \{\mathbf{F}, \mathbf{P}\}, \tag{28}$$

with

$$P_{\mu\nu}^{\sigma\sigma'} = \sum_i C_{\mu i}^\sigma C_{\nu i}^{\sigma'*}. \tag{29}$$

We may cast the rank-2 spinor structure of $\mathbf{F}$ and $\mathbf{P}$ (Eq. (B.5b)) into a simple form

$$\mathbf{F} = \mathbf{F}^S \otimes \boldsymbol{I}_2 + \sum_k \mathbf{F}^k \otimes \boldsymbol{\sigma}_k, \tag{30}$$

$$\mathbf{P} = \mathbf{P}^S \otimes \boldsymbol{I}_2 + \sum_k \mathbf{P}^k \otimes \boldsymbol{\sigma}_k, \tag{31}$$

where

$$\mathbf{F}^S = \mathbf{h}^S + \mathbf{J}[\mathbf{P}^S] + \mathbf{V}^{xc,S}, \tag{32}$$

$$\mathbf{F}^k = \mathbf{h}^k + \mathbf{V}^{xc,k}. \tag{33}$$

$\mathbf{J}$ is the Coulomb matrix,

$$J[\mathbf{P}^S]_{\mu\nu} = \sum_{\lambda\kappa} (\mu\nu|\lambda\kappa) P_{\lambda\kappa}^S, \tag{34}$$

where

$$(\mu\nu|\lambda\kappa) = \int \mathrm{d}^3\mathbf{r} \int \mathrm{d}^3\mathbf{r}' \frac{\chi_\mu(\mathbf{r})\chi_\nu(\mathbf{r})\chi_\lambda(\mathbf{r}')\chi_\kappa(\mathbf{r}')}{|\mathbf{r}-\mathbf{r}'|}, \tag{35}$$

$\{\mathbf{h}^S, \mathbf{h}^z, \mathbf{h}^y, \mathbf{h}^x\}$ are the components of the two-component relativistic core Hamiltonian transformed in the same manner as the spinor Fock matrix (Eq. (B.5b)). $\{\mathbf{V}^{xc,S}, \mathbf{V}^{xc,z}, \mathbf{V}^{xc,y}, \mathbf{V}^{xc,x}\}$ are the components of the exchange correlation potential, where, given the functional form of equation (16), takes the form

$$\mathbf{V}^{xc,I} = \mathbf{V}^{GGA,I} - c_x \mathbf{K}[\mathbf{P}^I] \quad I \in \{S, x, y, z\}, \tag{36}$$

where $\mathbf{K}$ is the exchange matrix of Hartree–Fock theory,

$$K[\mathbf{P}^I]_{\mu\nu} = \sum_{\lambda\kappa} (\mu\lambda|\nu\kappa) P_{\lambda\kappa}^I, \tag{37}$$

and

$$V_{\mu\nu}^{GGA,I} = \frac{\delta E_{\mathrm{xc}}^{GGA}}{\delta P_{\mu\nu}^I}. \tag{38}$$

Efficient algorithms for the evaluation of the $\mathbf{J}$ and $\mathbf{K}$ matrices are well understood and outside of the scope of this work. In the subsequent section, we will provide a detailed description of the practical evaluation of equation (38), for which the effective change of basis outlined in equations (30) and (31) will serve as a primary basis.

2.1 Assembly of $\mathbf{V}^{GGA}$ for spinor densities

In this section, we examine the integration and assembly of the E_{xc}^{GGA} dependent terms of the Kohn–Sham Fock

matrix using a spinor density. In general, the exchange correlation contribution to the electronic energy may be written as an integral over an exchange correlation (xc) integration kernel, f,

$$E_{\text{xc}}^{GGA}[\rho, \nabla\rho] = \int \mathrm{d}^3\mathbf{r}\ f(\{U(\mathbf{r})\}), \tag{39}$$

where we have introduced a set of auxiliary "U"-variables, $\{U(\mathbf{r})\}$, upon which the xc kernel depends. These need not be the density variables $(\rho, \nabla\rho)$ directly, which we will refer to as "V"-variables, $\{V(\mathbf{r})\}$, but rather have complete flexibility in functional form. In non-relativistic, spin-polarized density functional theory, these sets of variables may be defined as

$$\{V^{\text{col}}(\mathbf{r})\} = \{\rho^\alpha(\mathbf{r}), \rho^\beta(\mathbf{r}), \nabla\rho^\alpha(\mathbf{r}), \nabla\rho^\beta(\mathbf{r})\}, \tag{40}$$

and

$$\{U^{\text{col}}(\mathbf{r})\} = \{\rho^\alpha(\mathbf{r}), \rho^\beta(\mathbf{r}), \gamma^{\alpha\alpha}(\mathbf{r}), \gamma^{\alpha\beta}(\mathbf{r}), \gamma^{\beta\beta}(\mathbf{r})\}, \tag{41}$$

where

$$\gamma^{\sigma\sigma'}(\mathbf{r}) = \nabla\rho^\sigma(\mathbf{r}) \cdot \nabla\rho^{\sigma'}(\mathbf{r}). \tag{42}$$

The practical utility for the use of these two separate sets of variables is especially apparent in the context of two-component density functional theory as it allows for a simple retrofitting of standard xc functionals for relativistic calculations by simply redefining the transformations from the V variables of relativistic theory.

In the following, we will make use of the transformation of the spin blocked density of equation (24) to the variables $\{\rho^S, \rho^z, \rho^y, \rho^x\}$ via equation (B.5b). Defining the magnetization density as $\mathbf{m}(\mathbf{r}) = \{\rho^z(\mathbf{r}), \rho^y(\mathbf{r}), \rho^x(\mathbf{r})\}$, non-collinear analogues for equations (40) and (41) may be defined as

$$\{V^{NC}(\mathbf{r})\} = \{\rho^S(\mathbf{r}), \mathbf{m}(\mathbf{r}), \nabla\rho^S, \nabla\mathbf{m}(\mathbf{r})\}, \tag{43}$$

$$\{U^{NC}(\mathbf{r})\} = \{n^+(\mathbf{r}), n^-(\mathbf{r}), \gamma^{++}(\mathbf{r}), \gamma^{+-}(\mathbf{r}), \gamma^{--}(\mathbf{r})\}, \tag{44}$$

where we have used NC to denote non-collinearity. The connection between $\{U^{\text{col}}\}$ and $\{U^{NC}\}$ is clear by making the substitution $\alpha \leftrightarrow +$ and $\beta \leftrightarrow -$. $\{V^{\text{col}}\}$ and $\{V^{NC}\}$ may be related by recognizing $\{\rho^\alpha, \rho^\beta\}$ as the diagonal contributions of the spinor density, and thus

$$\{\rho^\alpha(\mathbf{r}), \rho^\beta(\mathbf{r})\} \mapsto \{\rho^S(\mathbf{r}), \mathbf{m}^{\text{col}}(\mathbf{r})\}, \tag{45}$$

where $\mathbf{m}^{\text{col}}(\mathbf{r}) = \{\rho^z(\mathbf{r}), 0, 0\}$. Given the components of the spinor density matrix, spatial evaluation of the V-variables is given by

$$\rho^I(\mathbf{r}) = \sum_{\mu\nu} \text{Re}[P^I_{\mu\nu}]\chi_\mu(\mathbf{r})\chi_\nu(\mathbf{r}), \tag{46}$$

$$\nabla\rho^I(\mathbf{r}) = 2\sum_{\mu\nu} \text{Re}[P^I_{\mu\nu}]\chi_\mu(\mathbf{r})\nabla\chi_\nu(\mathbf{r}), \tag{47}$$

where $\text{Re}[x]$ denotes the real part of x. Remark that the evaluation of $\{V(\mathbf{r})\}$ may then be practically evaluated using strictly real arithmetic.

Given a transformation, $\{V^{NC}(\mathbf{r})\} \mapsto \{U^{NC}_I(\mathbf{r})\}$, it is possible to perform practical density functional calculations using standard implementations of collinear xc functionals, such as those provided by `libxc` [100,101]. However, defining such a transformation is not a trivial task, as the added spin degrees of freedom in the non-collinear spinor density and Fock matrix must obey to stricter conditions than their collinear counterparts, such as orientation invariance and adhering to the zero-torque theorem for the xc potential [88]. Several definitions of the generalized density variables have been proposed [79,82–84,102]. In this work, we utilize the transformation method which meets such conditions from reference [53]

$$n^\pm(\mathbf{r}) = \frac{1}{2}\rho^S(\mathbf{r}) \pm \frac{1}{2}|\mathbf{m}(\mathbf{r})|, \tag{48a}$$

$$\gamma^{\pm\pm}(\mathbf{r}) = \frac{1}{4}\nabla\rho^S(\mathbf{r}) \cdot \nabla\rho^S(\mathbf{r}) + \frac{1}{4}\sum_k \nabla\rho^k(\mathbf{r}) \cdot \nabla\rho^k(\mathbf{r}) \pm \frac{f_\nabla(\mathbf{r})}{2}\sqrt{\sum_k D^{Sk}(\mathbf{r})^2}, \tag{48b}$$

$$\gamma^{+-}(\mathbf{r}) = \frac{1}{4}\nabla\rho^S(\mathbf{r}) \cdot \nabla\rho^S(\mathbf{r}) - \frac{1}{4}\sum_k \nabla\rho^k(\mathbf{r}) \cdot \nabla\rho^k(\mathbf{r}), \tag{48c}$$

where

$$f_\nabla(\mathbf{r}) = \text{sgn}\left(\nabla\rho^S(\mathbf{r}) \cdot \left(\sum_k \nabla\rho^k(\mathbf{r}) \cdot \rho^k(\mathbf{r})\right)\right), \tag{49}$$

$$D^{IJ}(\mathbf{r}) = \nabla\rho^I(\mathbf{r}) \cdot \nabla\rho^J(\mathbf{r}). \tag{50}$$

Using this set of transformations, we may define an electronic energy and Fock matrix which has no dependence on the global orientation of $\mathbf{m}(\mathbf{r})$ and which satisfies the zero torque theorem (see Appendices A and B) for the exchange correlation potential also in the GGA framework. Instead of treating all components of spin-magnetization vector on equal footing, Vignale and coworkers introduced a formalism that weighs transverse and longitudinal spin-magnetization components differently [103]. The formalism used here has been shown to be satisfactory for systems with either weak or significantly inhomogeneous spin polarization [83,84,103] and for non-collinear TDDFT calculations [53].

In the limit of small $\mathbf{m}(\mathbf{r})$ ($|\mathbf{m}(\mathbf{r})| < 10^{-12}$, in this work), the transformations outlined in equation (48) yield numerically unstable expressions for the exchange correlation potential [53]. Thus one must define another set of transformations for practical implementations of non-collinear DFT to ensure proper convergence in the limit of small $\mathbf{m}(\mathbf{r})$. In summary, this change for small $\mathbf{m}(\mathbf{r})$ may be described by the following substitutions in

equation (48),

$$|\mathbf{m}(\mathbf{r})| \mapsto m_s(\mathbf{r}) = \frac{1}{3}\sum_k \rho^k(\mathbf{r}), \tag{51a}$$

$$\sqrt{\sum_k \left(D^{Sk}(\mathbf{r})\right)^2} \mapsto \nabla\rho^S(\mathbf{r}) \cdot \nabla m_s(\mathbf{r}). \tag{51b}$$

Using these mappings ensures no orientation dependence of **m** while maintaining numerical stability in the resulting expression for the xc potential. While equation (51) formally violates the zero torque theorem, its influence on the over all nature of the electronic density has been shown to be negligible [53].

Differentiating equation (39) with respect to the elements of the density matrix, we obtain for equation (38)

$$\begin{aligned} V_{\mu\nu}^{GGA,I} &= \sum_{\Gamma\Gamma'} \int \mathrm{d}^3\mathbf{r}\, \frac{\partial f}{\partial U^{\Gamma}(\mathbf{r})} \frac{\partial U^{\Gamma}(\mathbf{r})}{\partial V^{\Gamma'}(\mathbf{r})} \frac{\partial V^{\Gamma'}(\mathbf{r})}{\partial P^I_{\mu\nu}} \\ &= \int \mathrm{d}^3\mathbf{r} V_{\mu\nu}^{GGA,I}(\mathbf{r}), \end{aligned} \tag{52}$$

where the partial derivatives of f are the same as in collinear DFT, and the partial derivatives of $\{V(\mathbf{r})\}$ may be identified through differentiating equation (46) for a particular spin component. We refer the reader to the Appendix of reference [53] for explicit expressions for the partial derivatives of $\{U(\mathbf{r})\}$.

In practice, equations (39) and (52) are evaluated numerically using a molecular quadrature scheme [12–18],

$$E_{\mathrm{xc}^{\mathrm{GGA}}}[\rho, \nabla\rho] \approx \sum_i w(\mathbf{r}_i) f(\{U(\mathbf{r}_i)\}), \tag{53}$$

$$V_{\mu\nu}^{GGA,I} \approx \sum_i w(\mathbf{r}_i) V_{\mu\nu}^{GGA,I}(\mathbf{r}_i), \tag{54}$$

where $\{w(\mathbf{r}_i)\}$ is a set of quadrature weights. In this work, we utilize the Becke multi-center numerical integration scheme [12], where the integral is evaluated on series of overlapping atomic centered grids, transformed, through their weights, into "fuzzy", overlapping, and analytically continuous cells instead. We also refer the reader to a more thorough discussion regarding specific details [12,16]. The evaluation of equation (53) is straight forward as it is a scalar function. In the spirit of the intermediates used in reference [18], by substituting the definitions of the partial derivatives of the U and V variables, we arrive at a concise expressions for assembly of equation (54)

$$V_{\mu\nu}^{GGA,I} = \sum_i Z_\mu^I(\mathbf{r}_i)\chi_\nu(\mathbf{r}_i) + Z_\nu^I(\mathbf{r}_i)\chi_\mu(\mathbf{r}_i), \tag{55}$$

$$Z_\mu^I(\mathbf{r}) = w(\mathbf{r}) \left(\frac{1}{2}\mathcal{Z}_\rho^I(\mathbf{r})\chi_\mu(\mathbf{r}) + \sum_\xi \mathcal{Z}_{\nabla,\xi}^I(\mathbf{r})\nabla_\xi\chi_\mu(\mathbf{r}) \right), \tag{56}$$

where $\xi \in \{x, y, z\}$ and

$$\mathcal{Z}_\rho^I = \frac{\partial f}{\partial \rho^I} \tag{57a}$$

$$\mathcal{Z}_{\nabla,\xi}^I = \frac{\partial f}{\partial \nabla_\xi \rho^I} \tag{57b}$$

$$\mathcal{Z}_\rho^I = \frac{1}{2} \begin{cases} \left(\dfrac{\partial f}{\partial n^+} + \dfrac{\partial f}{\partial n^-} \right) & I = S \\ \left(\dfrac{\partial f}{\partial n^+} - \dfrac{\partial f}{\partial n^-} \right) K^I & I \neq S, \end{cases} \tag{58a}$$

$$\mathcal{Z}_{\nabla,\xi}^I = \frac{1}{2} \begin{cases} \nabla_\xi\rho^S \left(\dfrac{\partial f}{\partial \gamma^{++}} + \dfrac{\partial f}{\partial \gamma^{+-}} + \dfrac{\partial f}{\partial \gamma^{--}} \right) \\ \quad + \sum_k \nabla_\xi\rho^k H^k \left(\dfrac{\partial f}{\partial \gamma^{++}} - \dfrac{\partial f}{\partial \gamma^{--}} \right) & I = S \\ \nabla_\xi\rho^S H^I \left(\dfrac{\partial f}{\partial \gamma^{++}} - \dfrac{\partial f}{\partial \gamma^{--}} \right) \\ \quad + \nabla_\xi\rho^I \left(\dfrac{\partial f}{\partial \gamma^{++}} - \dfrac{\partial f}{\partial \gamma^{+-}} + \dfrac{\partial f}{\partial \gamma^{--}} \right) & I \neq S, \end{cases} \tag{58b}$$

where we have dropped the explicit dependence on **r** for brevity. To consolidate the transformation rules of equations (48) and (51), we now define

$$K^I = \begin{cases} \dfrac{\rho^I}{|\mathbf{m}|} & (\text{Significant } \mathbf{m}) \\ \dfrac{1}{3} & (\text{Small } \mathbf{m}), \end{cases} \tag{59a}$$

$$H^I = \begin{cases} \dfrac{f_\nabla D^{SI}}{\sqrt{\sum_k \left(D^{Sk}\right)^2}} & (\text{Significant } \mathbf{m}) \\ \dfrac{f_\nabla}{3} & (\text{Small } \mathbf{m}). \end{cases} \tag{59b}$$

3 Implementation

On modern computing architectures, there are three primary facets one must consider when developing high–performance scientific software: parallelism, cache utilization, and exploitation of micro-architecture specific floating point operations (μ-ops) such as single instruction–multiple data (SIMD) and fused multiply–add (FMA) operations. We refer the reader to the work of Goto and Geijn [104] for an excellent discussion of these considerations in the context of matrix operations. In the context of density functional theory, maximal exploitation of computational cache and μ-ops is achieved through batching groups of integration points together to maximize screening capability and memory contingency. There

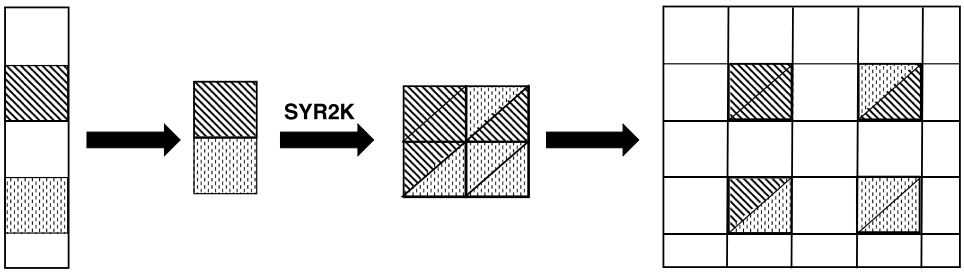

Fig. 1. Pictorial representation of the screening and updating scheme for each batch. A list of significant basis functions in the batch (colored patterns in the figure), is selected and than used for integration. The collection of sub-matrices for the entire batch is integrated by symmetric rank-2k update routine (SYR2K) and inserted in the final result. See text for a more detailed discussion.

exist many batching schemes for various molecular integration quadratures in the literature [12–18]. We provide the following discussion without loss of generality.

As the point-wise function evaluations required for numerical integration are completely independent, it constitutes what is called an *embarrassingly parallel task*, i.e. no communication is required between the independent operations and thus one should expect near linear speedup with the number of processors used. In the context of electronic structure theory, the final two facets can usually be addressed through the use of highly optimized linear algebra software, such as the optimized BLAS (basic linear algebra subroutines) implementations offered OpenBLAS [105,106] BLIS [107] and Intel–MKL [108]. However, blind application of such software without careful consideration will often yield sub-optimal results, thus it is often the case that one must perform some level of algorithmic rearrangement to maximally utilize such capability. To demonstrate this point, we examine the assembly of the exchange correlation potential in equation (55). One may immediately recognize that the operation on the left of equation (55) is a sum over symmetric rank-2 updates (SYR2) of column vectors, $\mathbf{z}$ and $\boldsymbol{\chi}$, i.e.

$$\mathbf{V}^{GGA,I} = \sum_i \mathbf{z}_i^I \boldsymbol{\chi}_i^T + \boldsymbol{\chi}_i \left(\mathbf{z}_i^I\right)^T, \tag{60}$$

where $\mathbf{z}_i^I$ and $\boldsymbol{\chi}_i$ are of length of the number of basis functions, N_b. While equation (60) is a valid scheme for the assembly of equation (55), for large N_b this scheme will be drastically sub-optimal. This is due to the fact that, for large N_b, $\mathbf{V}^{GGA,I}$, $\mathbf{z}_i^I$ and $\boldsymbol{\chi}_i$ occupy a significant portion of the computational caches for each point. This means that the probability of the program attempting to access a memory address, i.e. an element of $\mathbf{z}_i^I$ or $\boldsymbol{\chi}_i$, between integration points and finding that it does not currently reside in the cache, i.e. a "cache miss", is rather high relative to other memory access patterns. This yields a large degradation in performance as whenever a cache miss occurs, the program must then move that address in some manner to the cache from main memory before it can perform any operations on it. Moving data to and from main memory is disproportional more expensive than floating point operations, thus it must be kept to a minimum to obtain optimal efficiency.

We may instead factor out a portion of the sum in equation (60) such that we may partition it into sum over batch of points (S_j). In detail, we use the macrobatch approach [16], where the grid points of each atoms are arranged in Lebedev spheres [109] of several radii, for the numerical integration of the exchange correlation potential,

$$\begin{aligned}\mathbf{V}^{GGA,I} &= \sum_{S_j \in S} \left(\sum_{i \in S_j} \mathbf{z}_i^I \boldsymbol{\chi}_i^T + \boldsymbol{\chi}_i \left(\mathbf{z}_i^I\right)^T \right) \\ &= \sum_{S_j \in S} \mathbf{Z}^{I(j)} \left(\mathbf{X}^{(j)}\right)^T + \mathbf{X}^{(j)} \left(\mathbf{Z}^{I(j)}\right)^T, \end{aligned} \tag{61}$$

where

$$\mathbf{Y}^{(j)} = \begin{bmatrix} \mathbf{y}_1 & \mathbf{y}_2 & \cdots & \mathbf{y}_i & \cdots & \mathbf{y}_{|S_j|} \end{bmatrix} \quad \forall i \in S_j, \tag{62}$$

and $\mathbf{y}$ is either $\mathbf{z}$ or $\boldsymbol{\chi}$. Equation (61) is a sum over symmetric rank-$2k$ updates (SYR2K), where $k = |S_j|$. By tuning k, one improves caching behavior dramatically. This is due to the fact that optimized implementations of SYR2K operations utilized efficient block operations to optimize the flow of data to and from the computational caches. Similar schemes may developed for the evaluation of the V variables (Eq. (46)) over batches using optimized matrix–matrix multiplication routines. However, while the caching behavior is improved with increasing k, this is not the only consideration one needs take into account when partitioning the integration grid into batches.

The scheme in equation (61) may be further improved by recognizing the fact that the basis functions typically used for molecular calculations carry a degree of spatial locality. A pictorial representation of the screening and updating scheme is given in Figure 1. For each batch, we create a list of basis functions that effectively overlaps it (colored subset of basis functions in Fig. 1). This list of significant basis functions will be different for each batch, but the number of basis functions in each list becomes independent of size for sufficiently large molecules, given the spatial localization nature of Gaussian atomic centered basis sets. This reduced list of basis, evaluated for all points in the batch, is stored in contiguous blocks of memory, and used (along with the corresponding submatrices of the density-matrix, when required) for the evaluation

of the potential, $\mathbf{Z}$ (see Eq. (56)), by exploiting a subsequential series of vectorized operations. An important note here is that the maximum values for the batch of basis functions, $\chi_{\max}(\text{batch})$, and potential, $Z_{\max}(\text{batch})$, can be used to screen the entire contribution of the points in the batch to the integration. In this case, the integration can move to the next batch, avoiding the rank-2k update, that is the computationally most expensive part of the process, without loosing accuracy. Otherwise, recognizing that $\mathbf{Z}$ and $\mathbf{X}$ exhibit the same sparsity pattern, we may define

$$\tilde{\mathbf{V}}^{GGA,I}_{(j)} = \tilde{\mathbf{Z}}^{I(j)} \left(\tilde{\mathbf{X}}^{(j)}\right)^T + \tilde{\mathbf{X}}^{(j)} \left(\tilde{\mathbf{Z}}^{I(j)}\right)^T, \tag{63}$$

where moieties denoted with a tilde are the packed quantities where only the basis functions which have been chosen to be evaluated for the batch are represented. The packed $\tilde{\mathbf{V}}^{\text{GGA,I}}_{(j)}$ may then be used to update the full $\mathbf{V}^{\text{GGA,I}}$ by mapping its elements to those in the full basis dimension.

4 Discussion

4.1 Validation

Molecular systems characterized by geometrically frustrated conformations have been used to gauge the reliability of the presented implementation, since generalized-KS and X2C-KS, unlike U-KS, methods are capable to support the broken $\hat{S}_z$ symmetry that minimizes Pauli repulsion [82–84,90,110–114]. Thus, we examined a series of neutral hydrogen rings, ranging from 3 to 8 hydrogen atoms, that have already been proved to show broken symmetry solutions within generalized Hartree–Fock theory [114]. The used conformations have 1 Å spaced hydrogen atoms and only the odd-membered rings will be geometrically frustrated. All hydrogen rings electronic structure were obtained by solving the presented X2C-KS equation in open-source `ChronusQ` [115] electronic structure software using the hybrid Becke, 3-parameter, Lee-Yang-Parr (B3LYP) density functional [116–118] with a 6-311+g** basis, since it is required to include the polarization of hydrogenic s-functions [114]. Qualitatively, X2C-KS solutions are given in Figure 2, where both the spin and the charge densities are reported, respectively. The spin density in the non-collinear approach is a mapping of the 2-norm of the spin magnetization vector onto the total density [79], ensuring the spin density to be positive and always real, and the charge density is a mapping of the electrostatic potential to the total density. For even numbered rings, the anti-ferromagnetic spin distribution can be observed, aside from the six rings (where the closed shell solution is the most stable one according to the $2n+1$ rule for Möbius-like periodicity). For odd membered rings, the Möbius-like periodicity of magnetization ordering in X2C-KS results can be inspected by the totally symmetric distribution of the spin density throughout the structure in Figure 2. This symmetric distribution can not be supported by collinear solutions [114] which are constrained to be eigenfunctions of $\hat{S}_z$. Thus, X2C-B3LYP is able to

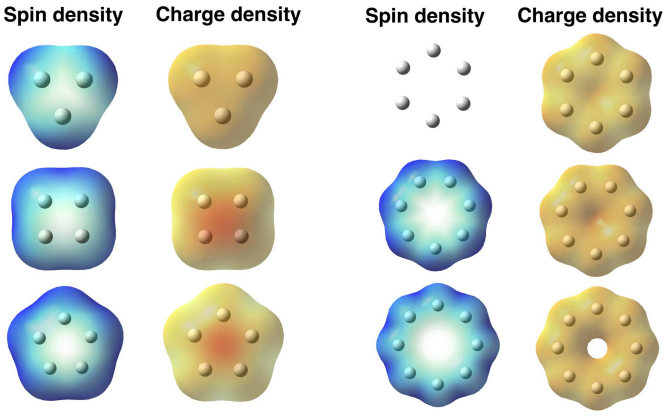

Fig. 2. X2C-B3LYP 6-311+g** spin and charge densities for hydrogen rings sizes 3–8. The spin density is represented as the 2-norm of the magnetization vector at each point in space (left, in blue largest magnitude), and the charge density as the electrostatic potential mapped to the total density (right, in red largest electronic population).

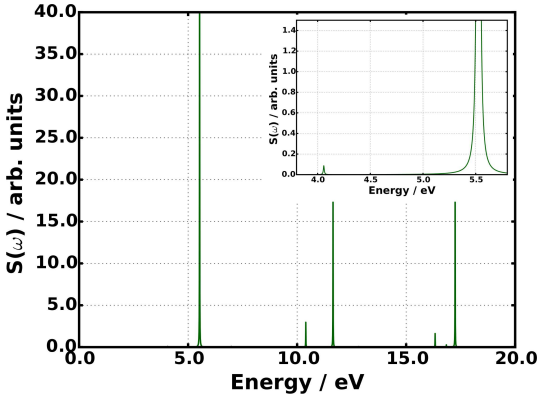

Fig. 3. X2C-SVWN5 Sapporo-DKH3-DZP-2012, including diffuse-sp, computed optical absorption spectrum for Cd atom. An inset presenting the zoomed in region between 3.9 eV and 5.6 eV is reported in the upper right corner. A larger integration DFT grid was used (252 × 974 grid) to ensure better accuracy.

reproduce the expected symmetry of non-collinear results for odd membered rings [114], ensuring the reliability of the current implementation.

A second test was conducted to further validate the correct implementation of the X2C-DFT framework. The valence excitations of a group 12 transition metal atom, Cd, were computed via real-time X2C-TDDFT. [28,119–123]. The procedure presented in reference [28] was employed to propagate the X2C-TDDFT equations in time containing the external electric field perturbation. In brief, calculations were performed using the SVWN5 [124,125] density functional with the Sapporo-DKH3-DZP-2012 Gaussian basis set including diffuse-sp functions [126]. After converging the ground state density, the system was perturbed with an electric dipole delta pulse corresponding to $\kappa = 0.0001$ au along each unique Cartesian axis. Each real-time dynamics was propagated using a time step of 0.0012 fs for 50 fs. Energy was

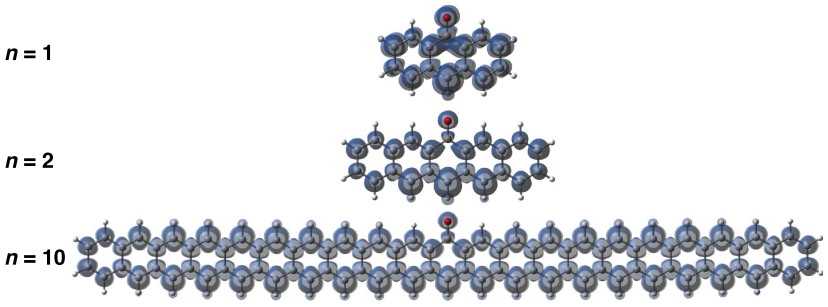

Fig. 4. X2C-B3LYP 6-311+G(2*d*,*p*) spin densities for phenoxy radicals with increasing number of symmetrical fused benzene rings ($n = 1$–10, where n represents the number of fused benzene rings on each side). The spin density (here the 0.001 iso-surface) is obtained as the 2-norm of the magnetization vector at each point in space.

conserved to at least 10^{-8} au. The optical absorption spectrum was obtained by plotting the isotropic dipole strength function, $S(\omega)$, proportional to the imaginary component of the trace of the frequency dependent polarizability, via the Fourier transform of the time-dependent electric dipole moment ($\mu(\omega)$) parallel to the polarization of the electric field perturbation according the following

$$S(\omega) \propto \sum_{\alpha=x,y,z} \mathrm{Tr}\left[\omega \cdot \mathrm{Im}\frac{\mu_\alpha(\omega)}{\kappa_\alpha}\right]. \tag{64}$$

To accelerate convergence of the Fourier transform, a Padé transformation scheme was utilized [127]. The electric dipole response was exponentially damped so as to give each peak a Lorentzian line shape with full-width half-max of 0.01 eV. The spectrum is reported in Figure 3. The spin-forbidden singlet, $^1S_0$, to triplet, $^3P_1$ states, (∼4.06 eV) and spin-allowed singlet, $^1S_0$, to singlet, $^1P_1$, (∼5.53 eV) transitions can be easily assigned based on the relative intensities in Figure 3 (see inset). Real-time X2C-TDDFT method can only detect electronically allowed transitions, thus singlet to triplet transitions (appearing at ∼4.06 eV) can be only observed since the X2C Hamiltonian includes spin-orbit couplings which allow the otherwise spin-forbidden transitions to become weakly allowed. The presented results are also in nice agreement with previously computed values including relativistic effects, further ensuring the accuracy of the current implementation [28,51,128–132].

4.2 Performances

After we have checked the reliability and presented the schematics of the integration scheme, we focus on the performances of the method. All the following tests presented are performed without exploiting symmetry using B3LYP/6–311+G(2*d*,*p*) theory level and atomic centered grids resulting as the product of a radial and angular quadrature, using 100 Euler–Maclaurin [14], and 302 Lebedev ($l = 29$) [109] grid points, respectively (100 × 302 grid). All calculations were performed using Intel Haswell compute nodes (14×2 Intel®Xeon E5–2680 v4 CPUs @ 2.40 GHz, 32k L1 cache, 256k L2 cache, 35840k L3 cache). All times refer to the combined wall time for the numerical evaluation of E_{XC} and the matrix elements $V^{\mathrm{GGA,I}_{\mu\nu}}$,

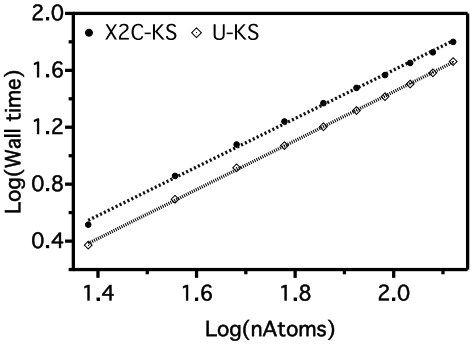

Fig. 5. Wall timings in seconds as a function of the total number of atoms in the systems for the evaluation of the E_{XC} and the matrix elements $X_{\mu\nu}$ in one SCF step (as average over 5 steps, 6–311+G(2d,p), 100 × 302 grid. Both the U-KS, empty diamonds, and X2C-KS, filled circles, are reported for comparison. A linear fit in this log-log scale is performed to show the similar scaling for the two different integration. The two lines show an identical slope and the X2C-KS is only ∼40% more expensive compared to the UKS.

(Eqs. (53) and (54)) for each self consistent field (SCF) step (as average over 5 steps). The scaling of the numerical integration with respect to increasing system sizes is investigated first by measuring wall timings on a series of phenoxy radicals with increasing number of symmetrical fused benzene rings ($n = 1$–10). These systems have been chosen, since they present a delocalized spin-density over the entire molecule (see Fig. 4) for all values of n. This is very important, since the screening based on the different components of the density can be very large in regions showing zero magnetization density. Wall times are shown in Figure 5 as function of the total number of atoms in the systems for both the U-KS and X2C-KS implementations. The scaling factors are similar for both U-KS and X2C-KS integration (see the parallel fitted lines in the figure), showing how the X2C-KS integration does not show any consistent computational overhead in the $V^{\mathrm{GGA,I}_{\mu\nu}}$ integration with respect to the common U-KS integration. Finally, by employing the largest phenoxy radical of the series ($n = 10$), the same wall times are recorded as function of increasing MPI processes across different computational nodes (for 1, 2, 4, 8, 12 nodes, for a total of 28, 56, 112, 224, 336 CPUs) and reported

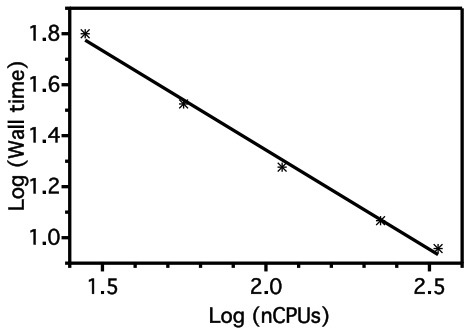

Fig. 6. Wall timings in seconds as function of increasing computational CPUs of the E_{XC} and the matrix elements $X_{\mu\nu}$ for each SCF step (as average over 5 steps, 6–311+G(2*d*,*p*), 100 × 302 grid, 2619 basis functions). A linear fit, –1.01 slope, is also represented as full line.

in Figure 6. The implemented algorithm presents linear (−1.01) with increasing number of CPUs, as can be expected since the integration over different atomic centers can be easily independently performed across different computing nodes.

5 Conclusions

In this work, we presented an integration and assembly strategy, using a two-component spinor density, for efficient evaluation of the exchange correlation term using localized basis functions. The presented formulation is suitable to exploit parallelism along with optimal cache utilization and micro-architecture specific floating point operations. This leads to the evaluation of exchange correlation contributions with matrices of optimal sizes. We also show that the proper choice of auxiliary variables correctly give rise to nonzero local torque of the xc magnetic field on the magnetization while maintaining net zero global torque, as is expected from the exact functional. Several tests were used to validate the reliability and the performance of the proposed strategy. This approach can help to extend the applicability of relativistic two-component DFT to systems of large size (>100 atoms).

Author contribution statement

Numerical integration engine for the relativistic two-component DFT was developed by AP. DBW developed the fast quaternion and complex arithmetics. AP, DBW, and TFS carried out computational tests and benchmarks. DBW, SC and XL were responsible for the underlying mathematics and proofs.

The development of the relativistic two-component DFT method is funded by the US Department of Energy (DE-SC0006863 to XL). This work was facilitated though the use of advanced computational, storage, and networking infrastructure provided by the Hyak supercomputer system funded by the STF at the University of Washington and the National Science Foundation (MRI-1624430).

Appendix A: Proof of zero torque theorem using generalized density variables

In this Appendix, we validate that the zero torque theorem for the xc magnetic field is satisfied in the generalized gradient approximation given the transformation rules of equation (48). The local torque does not need to vanish identically at every point in space and this local contribution is required to obtain accurate spin dynamics and a proper time-evolution of the magnetization [53,82–84,88,89]. The local torque of the xc magnetic field is the tensor field defined by [88]

$$\mathscr{T}_i(\mathbf{r}) = \sum_{jk} \varepsilon_{ijk} \rho^j(\mathbf{r}) B^k_{GGA}(\mathbf{r}), \tag{A.1}$$

where $\varepsilon_{\mathrm{ijk}}$ is the rank-3 Levi–Civita tensor and the xc magnetic field is given by

$$B^k_{\mathrm{GGA}}(\mathbf{r}) = \frac{\delta E_{\mathrm{GGA}}[\rho, \nabla\rho]}{\delta \rho^k(\mathbf{r})}. \tag{A.2}$$

From equation (A.1), we may define the global torque of the xc magnetic field as

$$\mathscr{T}_i^{\mathrm{global}} = \int \mathrm{d}^3\mathbf{r}\ \mathscr{T}_i(\mathbf{r}). \tag{A.3}$$

Remark that the set of U variables in equation (48) is partitioned by those variables which depend on $\mathbf{m}(\mathbf{r})$ and those which depend on $\nabla\mathbf{m}(\mathbf{r})$. Recognizing that our choice of U variables are local functions and applying the Euler–Lagrange formula for functional derivatives to equation (A.2), we obtain

$$\begin{aligned} B^k_{\mathrm{GGA}}(\mathbf{r}) &= \frac{\partial f}{\partial \rho^k(\mathbf{r})} - \nabla \cdot \frac{\partial f}{\partial \nabla \rho^k(\mathbf{r})} \\ &= B^{(\rho),k}_{\mathrm{GGA}}(\mathbf{r}) - B^{(\nabla),k}_{\mathrm{GGA}}(\mathbf{r}), \end{aligned} \tag{A.4}$$

where

$$B^{(\rho),k}_{\mathrm{GGA}}(\mathbf{r}) = \frac{\partial f}{\partial n^+(\mathbf{r})}\frac{\partial n^+(\mathbf{r})}{\partial \rho^k(\mathbf{r})} + \frac{\partial f}{\partial n^-(\mathbf{r})}\frac{\partial n^-(\mathbf{r})}{\partial \rho^k(\mathbf{r})}, \tag{A.5}$$

$$\begin{aligned} B^{(\nabla),k}_{\mathrm{GGA}}(\mathbf{r}) = \nabla \cdot \Bigg(&\frac{\partial f}{\partial \gamma^{++}(\mathbf{r})}\frac{\partial \gamma^{++}(\mathbf{r})}{\partial \nabla \rho^k(\mathbf{r})} + \frac{\partial f}{\partial \gamma^{+-}(\mathbf{r})}\frac{\partial \gamma^{+-}(\mathbf{r})}{\partial \nabla \rho^k(\mathbf{r})} \\ &+ \frac{\partial f}{\partial \gamma^{--}(\mathbf{r})}\frac{\partial \gamma^{--}(\mathbf{r})}{\partial \nabla \rho^k(\mathbf{r})}\Bigg). \end{aligned} \tag{A.6}$$

We refer the reader to the Appendix of reference [53] for explicit expressions for the partial derivatives of $\{U^{NC}(\mathbf{r})\}$ given by equation (43). Thus, the local and global torque expressions may also be similarly as they are linear in $\mathbf{B}_{\mathrm{GGA}}(\mathbf{r})$,

$$\mathscr{T}_i(\mathbf{r}) = \mathscr{T}_i^{\rho}(\mathbf{r}) + \mathscr{T}_i^{\nabla}(\mathbf{r}), \tag{A.7}$$

$$\mathscr{T}_i^{\rho}(\mathbf{r}) = \sum_{\mathrm{jk}} r\varepsilon_{\mathrm{ijk}} \rho^j(\mathbf{r}) B^{(\rho),k}_{\mathrm{GGA}}(\mathbf{r}), \tag{A.8}$$

$$\mathscr{T}_i^{(\rho),\text{global}} = \int \mathrm{d}^3\mathbf{r}\ \mathscr{T}_i^{\rho}(\mathbf{r}), \tag{A.9}$$

$$\mathscr{T}_i^{\nabla}(\mathbf{r}) = \sum_{\text{jk}} \varepsilon_{\text{ijk}} \rho^j(\mathbf{r}) B_{\text{GGA}}^{(\nabla),k}(\mathbf{r}), \tag{A.10}$$

$$\mathscr{T}_i^{(\nabla),\text{global}} = \int \mathrm{d}^3\mathbf{r}\ \mathscr{T}_i^{\nabla}(\mathbf{r}). \tag{A.11}$$

To identify the local and global torque contributions from equation (A.5), we may consolidate it with the magnetization components of equation (57),

$$B_{\text{GGA}}^{(\rho),k}(\mathbf{r}) = \mathcal{Z}_{\rho}^{k}(\mathbf{r}) = \frac{1}{2}\left(\frac{\partial f}{\partial n^+(\mathbf{r})} - \frac{\partial f}{\partial n^-(\mathbf{r})}\right)\frac{\rho^k(\mathbf{r})}{|\mathbf{m}(\mathbf{r})|}. \tag{A.12}$$

Substituting into equation (A.8), we obtain,

$$\begin{aligned}\mathscr{T}_i^{\rho}(\mathbf{r}) &= \frac{1}{2}\left(\frac{\partial f}{\partial n^+(\mathbf{r})} - \frac{\partial f}{\partial n^-(\mathbf{r})}\right)\sum_{\text{jk}}\frac{\varepsilon_{\text{ijk}}\rho^j(\mathbf{r})\rho^k(\mathbf{r})}{|\mathbf{m}(\mathbf{r})|} \\ &= 0, \implies \mathscr{T}_i^{(\rho),\text{global}} = 0,\end{aligned} \tag{A.13}$$

where we have utilized the fact that $\sum_{\text{jk}} \varepsilon_{\text{ijk}}\rho^j(\mathbf{r})\rho^k(\mathbf{r}) = 0$. Thus the local torque contribution of this term is zero in all space, implying that its global torque contribution is zero as well.

Similarly, we may identify equation (A.6) with the magnetization components of equation (58),

$$B_{\text{GGA}}^{(\rho),k}(\mathbf{r}) = \sum_{\xi} \nabla_\xi \mathcal{Z}_{\nabla,\xi}^{k}(\mathbf{r}). \tag{A.14}$$

However, unlike equation (A.13), the torque arising from equation (A.14) is *not* zero in all space. We must them examine its global torque contribution,

$$\begin{aligned}\mathscr{T}_i^{(\nabla),\text{global}} &= \sum_{\text{jk}}\sum_{\xi}\varepsilon_{\text{ijk}}\int \mathrm{d}^3\mathbf{r}\ \rho^j(\mathbf{r})\ \nabla_\xi \mathcal{Z}_{\nabla,\xi}^{k}(\mathbf{r}) \\ &= -\sum_{\text{jk}}\sum_{\xi}\varepsilon_{\text{ijk}}\int \mathrm{d}^3\mathbf{r}\ \mathcal{Z}_{\nabla,\xi}^{k}(\mathbf{r})\left(\nabla_\xi\rho^j(\mathbf{r})\right).\end{aligned} \tag{A.15}$$

Here, we have integrated the first line by parts and utilized the fact that the density and its derivatives disappear at the boundary by definition. Substituting in the expressions from equation (58),

$$\begin{aligned}\mathscr{T}_i^{(\nabla),\text{global}} = -\frac{1}{2}\sum_{\text{jk}}\sum_{\xi}\varepsilon_{\text{ijk}}\int \mathrm{d}^3\mathbf{r}\ \nabla_\xi\rho^j(\mathbf{r}) \\ \times\left(\nabla_\xi\rho^S(\mathbf{r})H^k(\mathbf{r})\left(\frac{\partial f}{\partial\gamma^{++}(\mathbf{r})} - \frac{\partial f}{\partial\gamma^{--}(\mathbf{r})}\right)\right. \\ + \nabla_\xi\rho^k(\mathbf{r})\left(\frac{\partial f}{\partial\gamma^{++}(\mathbf{r})} - \frac{\partial f}{\partial\gamma^{+-}(\mathbf{r})}\right. \\ \left.\left. + \frac{\partial f}{\partial\gamma^{--}(\mathbf{r})}\right)\right) = 0,\end{aligned} \tag{A.16}$$

where we have used the following relations

$$\begin{aligned}&\nabla\rho^S(\mathbf{r})\cdot\nabla\rho^j(\mathbf{r})H^k(\mathbf{r}) = \nabla\rho^S(\mathbf{r})\cdot\nabla\rho^k(\mathbf{r})H^j(\mathbf{r}) \\ &\implies \sum_{\text{jk}}\varepsilon_{\text{ijk}}\nabla\rho^S(\mathbf{r})\cdot\nabla\rho^j(\mathbf{r})H^k(\mathbf{r}) = 0,\end{aligned} \tag{A.17}$$

$$\sum_{\text{jk}}\varepsilon_{\text{ijk}}\nabla\rho^j(\mathbf{r})\cdot\nabla\rho^k(\mathbf{r}) = 0. \tag{A.18}$$

Appendix B: Spin-Algebra over rank-2 spinors

In this section, we review the necessary spin-algebra to supplement the development of non-collinear electronic structure methods. Let $\mathbf{X}(2)$ be a rank-2 spinor, such that

$$\mathbf{X}(2) = \begin{bmatrix}\mathbf{X}(2)^{\alpha\alpha} & \mathbf{X}(2)^{\alpha\beta}\\ \mathbf{X}(2)^{\beta\alpha} & \mathbf{X}(2)^{\beta\beta}\end{bmatrix}, \tag{B.1}$$

where $\left\{\mathbf{X}(2)^{\sigma\sigma'} \in \text{GL}(\mathbb{C},N) \mid \sigma,\sigma' \in \{\alpha,\beta\}\right\}$ is a set of N-by-N complex matrices. Thus $\mathbf{X}(2) \in \text{GL}(\mathbb{C},N)\times\text{GL}(\mathbb{C},2)$. Choosing the standard basis of $\text{GL}(\mathbb{C},2)$ as $U^2\times U^2$, we may recast equation (B.1) as

$$\mathbf{X}(2) = \sum_{\sigma\sigma'}\mathbf{X}(2)^{\sigma\sigma'}\otimes\mathbf{e}_\sigma\otimes\mathbf{e}_{\sigma'} \qquad \mathbf{e}_\alpha = \begin{bmatrix}1\\0\end{bmatrix}, \quad \mathbf{e}_\beta = \begin{bmatrix}0\\1\end{bmatrix}, \tag{B.2}$$

and such is the standard treatment of spin non-collinearity in the literature, exemplified by treating the binary spin blocks of $\mathbf{X}(2)$ explicitly.

In this work, we rely on a change of basis to simplify the subsequent derivations and arithmetic in the development of non-collinear electronic structure. We choose the basis of the Pauli matricies (Eq. (3)), for which it may be shown that

$$\text{span}\left[\{\boldsymbol{I}_2,\boldsymbol{\sigma}_z,\boldsymbol{\sigma}_y,\boldsymbol{\sigma}_x\}\right] = \text{GL}(\mathbb{C},2), \tag{B.3}$$

i.e. $\{\boldsymbol{I}_2\}\cup\{\boldsymbol{\sigma}_k \mid k\in\{x,y,z\}\}$ forms a basis of $\text{GL}(\mathbb{C},2)$. Because the Pauli matricies form a basis for $\text{GL}(\mathbb{C},2)$, there must exist $\{\mathbf{X}(2)^S,\mathbf{X}(2)^z,\mathbf{X}(2)^y,\mathbf{X}(2)^x\}$ such that

$$\mathbf{X}(2) = \mathbf{X}(2)^S\otimes\boldsymbol{I}_2 + \sum_{k\in\{x,y,z\}}\mathbf{X}(2)^k\otimes\boldsymbol{\sigma}_k. \tag{B.4}$$

From the definitions in equation (3), we may define linear transformations ($\mathscr{T}$ and $\mathscr{T}^{-1}$) between the two bases and their components (the other being that of Eq. (B.2)),

$$\begin{bmatrix}\boldsymbol{I}_2\\ \boldsymbol{\sigma}_z\\ \boldsymbol{\sigma}_y\\ \boldsymbol{\sigma}_x\end{bmatrix} = \mathscr{T}\begin{bmatrix}\mathbf{e}_\alpha\otimes\mathbf{e}_\alpha\\ \mathbf{e}_\alpha\otimes\mathbf{e}_\beta\\ \mathbf{e}_\beta\otimes\mathbf{e}_\alpha\\ \mathbf{e}_\beta\otimes\mathbf{e}_\beta\end{bmatrix} \qquad \mathscr{T} = \begin{bmatrix}1 & 0 & 0 & 1\\ 1 & 0 & 0 & -1\\ 0 & -i & i & 0\\ 0 & 1 & 1 & 0\end{bmatrix}, \tag{B.5a}$$

$$\begin{bmatrix}\mathbf{X}(2)^S\\ \mathbf{X}(2)^z\\ \mathbf{X}(2)^y\\ \mathbf{X}(2)^x\end{bmatrix} = \mathscr{T}^{-T}\begin{bmatrix}\mathbf{X}(2)^{\alpha\alpha}\\ \mathbf{X}(2)^{\alpha\beta}\\ \mathbf{X}(2)^{\beta\alpha}\\ \mathbf{X}(2)^{\beta\beta}\end{bmatrix} \qquad \mathscr{T}^{-1} = \frac{1}{2}\mathscr{T}^\dagger. \quad \text{(B.5b)}$$

By resolving the identity with $\mathscr{T}$ in equation (B.2), we arrive at equation (B.4).

As a consequence of equations (B.4), (B.5a), (B.5b), and number of properties are immediately evident. Firstly, suppose there is another rank-2 spinor $\mathbf{Y}(2)$ described as in equation (B.4), the product of $\mathbf{X}(2)$ and $\mathbf{Y}(2)$ takes on a component form

$$\begin{aligned}\mathbf{XY}(2) = &\left(\mathbf{X}(2)^S\mathbf{Y}(2)^S + \sum_{k\in\{x,y,z\}}\mathbf{X}(2)^I\mathbf{Y}(2)^I\right)\otimes\boldsymbol{I}_2\\ &+\sum_{k\in\{x,y,z\}}\left(\mathbf{X}(2)^S\mathbf{Y}(2)^k + \mathbf{X}(2)^k\mathbf{Y}(2)^S\right.\\ &\left.+\sum_{j,l\in\{x,y,z\}} i\epsilon_{kjl}\mathbf{X}(2)^j\mathbf{Y}(2)^l\right)\otimes\boldsymbol{\sigma}_k. \quad \text{(B.6)}\end{aligned}$$

This form is convenient for a number of reasons, however in the context of electronic structure, equation (B.6) exhibits particular utility in the context of operator traces, i.e. property evaluation. Using the product ansatz of equation (B.6), we may write the trace of $\mathbf{X}(2)$ and $\mathbf{Y}(2)$ (denoted $\mathrm{Tr}[\mathbf{X}(2)\mathbf{Y}(2)]$) simply as

$$\begin{aligned}\mathrm{Tr}[\mathbf{X}(2)\mathbf{Y}(2)] = 2\Bigg(&\mathrm{Tr}\left[\mathbf{X}(2)^S\mathbf{Y}(2)^S\right]\\ &+\sum_{k\in\{x,y,z\}}\mathrm{Tr}\left[\mathbf{X}(2)^k\mathbf{Y}(2)^k\right]\Bigg). \quad \text{(B.7)}\end{aligned}$$

This simplicity of this expression is due to the fact that the trace operation over the Kronecker product is given by

$$\mathrm{Tr}[\mathbf{A}\otimes\mathbf{B}] = \mathrm{Tr}[\mathbf{A}]\mathrm{Tr}[\mathbf{B}], \quad \text{(B.8)}$$

and that the Pauli matricies are traceless with the exception of $\boldsymbol{I}_2$ which has a trace of 2.

Further, in the context of electronic structure theory, describing the Fock operator and electronic density as in equation (B.4) allows for a systematic treatment of all spin-restrictions (i.e. restricted, unrestricted and general) of single body electronic structure methods through a simple restriction of the populated Pauli matrix components, i.e.

$$\mathbf{F}(2) \sim \begin{cases}\mathbf{F}(2)^s, \mathbf{F}(2)^z, \mathbf{F}(2)^y, \mathbf{F}(2)^x & \text{GHF/GKS}\\ \mathbf{F}(2)^s, \mathbf{F}(2)^z & \text{UHF/UKS}\\ \mathbf{F}(2)^s & \text{RHF/RKS}\end{cases}, \quad \text{(B.9)}$$

and similarly for the electronic density, etc. From a practical perspective, electronic structure software which bases their methods on the spinor structure of equation (B.4) can generalize their code to work with any spin-restriction with only minor, systematic modifications.

References

1. P. Hohenberg, W. Kohn, Phys. Rev. **136**, B864 (1964)
2. W. Kohn, L.J. Sham, Phys. Rev. **140**, 1133 (1965)
3. E.K.U. Gross, J.F. Dobson, M. Petersilka, in *Density functional theory of time-dependent phenomena* (Springer, Berlin, Heidelberg, 1996), pp. 81–172
4. E. Runge, E.K.U. Gross, Phys. Rev. Lett. **52**, 997 (1984)
5. M.E. Casida, *Recent developments and applications in density functional theory* (Elsevier, Amsterdam, Netherlands, 1996)
6. M.A.L. Marques, E.K.U. Gross, Annu. Rev. Phys. Chem. **55**, 427 (2004)
7. K. Burke, J. Werschnik, E. Gross, J. Chem. Phys. **123**, 062206 (2005)
8. L.E. Ratcliff, S. Mohr, G. Huhs, T. Deutsch, M. Masella, L. Genovese, Wiley Interdiscip. Rev. Comput. Mol. Sci. **7**, e1290 (2017)
9. P. Ring, P. Schuck, *The nuclear many-body problem* (Springer Science and Business Media, Berlin, Germany, 2004)
10. I. Shavitt, R.J. Bartlett, *Many-body methods in chemistry and physics: MBPT and coupled-cluster theory* (Cambridge University Press, Cambridge, U.K., 2009)
11. T. Helgaker, P. Jorgensen, J. Olsen, *Molecular electronic-structure theory* (John Wiley and Sons, New York, NY, 2014)
12. A.D. Becke, J. Chem. Phys. **88**, 2547 (1988)
13. M.R. Pederson, K.A. Jackson, Phys. Rev. B **41**, 7453 (1990)
14. C.W. Murray, N.C. Handy, G.J. Laming, Mol. Phys. **78**, 997 (1993)
15. B.G. Johnson, in *Modern density functional theory: A tool for chemistry*, edited by J. Seminario, P. Politzer (Elsevier, Amsterdam, The Netherlands, 1995), Vol. 2, pp. 169–219
16. R. Stratmann, G.E. Scuseria, M.J. Frisch, Chem. Phys. Lett. **257**, 213 (1996)
17. A.M. Köster, R. Flores-Moreno, J.U. Reveles, J. Chem. Phys. **121**, 681 (2004)
18. A.M. Burow, M. Sierka, J. Chem. Theory Comput. **7**, 3097 (2011)
19. G. Lever, D.J. Cole, R. Lonsdale, K.E. Ranaghan, D.J. Wales, A.J. Mulholland, C.K. Skylaris, M.C. Payne, Phys. Chem. Lett. **5**, 3614 (2014)
20. C. Curutchet, B. Mennucci, Chem. Rev. **117**, 294 (2017)
21. G. Donati, A. Petrone, P. Caruso, N. Rega, Chem. Sci. **9**, 1126 (2018)
22. J. Hafner, C. Wolverton, G. Ceder, MRS Bull. **31**, 659 (2006)
23. J. Aarons, M. Sarwar, D. Thompsett, C.K. Skylaris, J. Chem. Phys. **145**, 220901 (2016)
24. A. Petrone, J.J. Goings, X. Li, Phys. Rev. B **94**, 165402 (2016)
25. G. Donati, D.B. Lingerfelt, A. Petrone, N. Rega, X. Li, J. Phys. Chem. A **120**, 7255 (2016)

26. N. Li, Z. Zhu, C.C. Chueh, H. Liu, B. Peng, A. Petrone, X. Li, L. Wang, A.K.Y. Jen, Adv. Energy Mater. **7**, 1601307 (2016)
27. D.C. Gary, A. Petrone, X. Li, B.M. Cossairt, Chem. Commun. **53**, 161 (2017)
28. J.J. Goings, J.M. Kasper, F. Egidi, S. Sun, X. Li, J. Chem. Phys. **145**, 104107 (2016)
29. D.B. Lingerfelt, D.B. Williams-Young, A. Petrone, X. Li, J. Chem. Theory Comput. **12**, 935 (2016)
30. A. Petrone, D.B. Lingerfelt, D.B. Williams-Young, X. Li, J. Phys. Chem. Lett. **7**, 4501 (2016)
31. A. Petrone, D.B. Williams-Young, D.B. Lingerfelt, X. Li, J. Phys. Chem. A **121**, 3958 (2017)
32. A.L. Buchachenko, V.L. Berdinsky, Chem. Rev. **102**, 603 (2002)
33. I. D'Amico, C.A. Ullrich, Phys. Status Solidi B **243**, 2285 (2006)
34. S. Sanvito, Chem. Soc. Rev. **40**, 3336 (2011)
35. P.J. Hore, H. Mouritsen, Annu. Rev. Biophys. **45**, 299 (2016)
36. E.K.U. Gross, R.M. Dreizler, *Relativistic density functional theory* (Springer US, Boston, MA, 1984), pp. 353–379
37. K.G. Dyall, K. Fægri, Jr., *Introduction to relativistic quantum chemistry* (Oxford University Press, Oxford, U.K., 2007)
38. P. Pyykkö, Annu. Rev. Phys. Chem. **63**, 45 (2012)
39. M. Reiher, A. Wolf, *Relativistic quantum chemistry: the fundamental theory of molecular science* (Wiley-VCH Verlag GmbH and Co. KGaA, Weinheim, Germany, 2015)
40. V.A. Soltamov, A.A. Soltamova, P.G. Baranov, I.I. Proskuryakov, Phys. Rev. Lett. **108**, 226402 (2012)
41. G. Thiering, A. Gali, Phys. Rev. B **96**, 081115 (2017)
42. J.R. Weber, W.F. Koehl, J.B. Varley, A. Janotti, B.B. Buckley, C.G. Van de Walle, D.D. Awschalom, Proc. Natl. Acad. Sci. U.S.A. **107**, 8513 (2010)
43. T.D. Ladd, F. Jelezko, R. Laflamme, Y. Nakamura, C. Monroe, J.L. OBrien, Nature **464**, 45 (2010)
44. D.D. Awschalom, L.C. Bassett, A.S. Dzurak, E.L. Hu, J.R. Petta, Science **339**, 1174 (2013)
45. T. Saue, T. Helgaker, J. Comput. Chem. **23**, 814 (2002)
46. F. Wang, W. Liu, J. Chin. Chem. Soc. **50**, 597 (2003)
47. D. Peng, W. Liu, Y. Xiao, L. Cheng, J. Chem. Phys. **127**, 104106 (2007)
48. T. Saue, Chem. Phys. Chem. **12**, 3077 (2011)
49. T. Saue, H.J.A. Jensen, J. Comput. Phys. **118**, 522 (2003)
50. J. Gao, W. Liu, B. Song, C. Liu, J. Chem. Phys. **121**, 6658 (2004)
51. R. Bast, H.J.A. Jensen, T. Saue, Int. J. Quant. Chem. **109**, 2091 2009
52. D. Williams-Young, F. Egidi, X. Li, J. Chem. Theory Comput. **12**, 5379 (2016)
53. F. Egidi, S. Sun, J.J. Goings, G. Scalmani, M.J. Frisch, X. Li, J. Chem. Theory Comput. **13**, 2591 (2017)
54. J. Gao, W. Zou, W. Liu, Y. Xiao, D. Peng, B. Song, C. Liu, J. Chem. Phys. **123**, 054102 (2005)
55. G. Vignale, in *Density functional theory* (Springer, Boston, MA, 1995), pp. 485–511
56. T. Kreibich, E.K.U. Gross, E. Engel, Phys. Rev. A **57**, 138 (1998)
57. W. Kohn, A. Savin, C.A. Ullrich, Int. J. Quant. Chem. **100**, 20 (2004)
58. F.A. Buot, J. Dobson, R. Dreizler, E. Engel, E. Gross, M. Petersilka, A. Rajagopal, in *Density functional theory II: relativistic and time dependent extensions* (Springer, Berlin, Germany, 1996), Vol. 2
59. G. Vignale, M. Rasolt, Phys. Rev. Lett. **59**, 2360 (1987)
60. P. Romaniello, P.L. de Boeij, J. Chem. Phys. **127**, 174111 (2007)
61. S. Sharma, S. Pittalis, S. Kurth, S. Shallcross, J.K. Dewhurst, E.K.U. Gross, Phys. Rev. B **76**, 100401 (2007)
62. N. Helbig, S. Kurth, S. Pittalis, E. Räsänen, E.K.U. Gross, Phys. Rev. B **77**, 245106 (2008)
63. A. Soncini, A.M. Teale, T. Helgaker, F.D. Proft, D.J. Tozer, J. Chem. Phys. **129**, 074101 (2008)
64. A.M. Lee, N.C. Handy, S.M. Colwell, J. Chem. Phys. **103**, 10095 (1995)
65. L.M. Sandratskii, Adv. Phys. **47**, 91 (1998)
66. C.A. Ullrich, J. Chem. Theory Comput. **5**, 859 (2009)
67. F.G. Eich, E.K.U. Gross, Phys. Rev. Lett. **111**, 156401 (2013)
68. J.E. Bates, F. Furche, J. Chem. Phys. **137**, 164105 (2012)
69. J.W. Furness, J. Verbeke, E.I. Tellgren, S. Stopkowicz, U. Ekström, T. Helgaker, A.M. Teale, J. Chem. Theory Comput. **11**, 4169 (2015)
70. C.R. Jacob, M. Reiher, Int. J. Quant. Chem. **112**, 3661 (2012)
71. F. Perez, F. Baboux, C.A. Ullrich, I. D'Amico, G. Vignale, G. Karczewski, T. Wojtowicz, Phys. Rev. Lett. **117**, 137204 (2016)
72. K. Capelle, G. Vignale, C.A. Ullrich, Phys. Rev. B **81**, 125114 (2010)
73. S. Karimi, F. Baboux, F. Perez, C.A. Ullrich, G. Karczewski, T. Wojtowicz, Phys. Rev. B **96**, 045301 (2017)
74. E. van Lenthe, E.J. Baerends, J.G. Snijders, J. Chem. Phys. **99**, 4597 (1993)
75. K.G. Dyall, J. Chem. Phys. **106**, 9618 (1997)
76. W. Kutzelnigg, W. Liu, J. Chem. Phys. **123**, 241102 (2005)
77. M. Iliaš, T. Saue, J. Chem. Phys. **126**, 064102 (2007)
78. J.J. Goings, F. Egidi, X. Li, Int. J. Quant. Chem. **118**, e25398 (2018)
79. C. Van Wüllen, J. Comput. Chem. **23**, 779 (2002)
80. F. Wang, T. Ziegler, J. Chem. Phys. **121**, 12191 (2004)
81. D. Peng, W. Zou, W. Liu, J. Chem. Phys. **123**, 144101 (2005)
82. J.E. Peralta, G.E. Scuseria, M.J. Frisch, Phys. Rev. B **75**, 125119 (2007)
83. G. Scalmani, M.J. Frisch, J. Chem. Theory Comput. **8**, 2193 (2012)
84. I.W. Bulik, G. Scalmani, M.J. Frisch, G.E. Scuseria, Phys. Rev. B **87**, 035117 (2013)
85. O. Fossgaard, O. Gropen, M.C. Valero, T. Saue, J. Chem. Phys. **118**, 10418 (2003)
86. H. Eschrig, V.D.P. Servedio, J. Comput. Chem. **20**, 23 (1999)
87. J. Anton, B. Fricke, E. Engel, Phys. Rev. A **69**, 012505 (2004)
88. K. Capelle, G. Vignale, B.L. Györffy, Phys. Rev. Lett. **87**, 206403 (2001)
89. K. Capelle, B.L. Gyorffy, Europhys. Lett. **61**, 354 (2003)
90. S. Sharma, J.K. Dewhurst, C. Ambrosch-Draxl, S. Kurth, N. Helbig, S. Pittalis, S. Shallcross, L. Nordström, E.K.U. Gross, Phys. Rev. Lett. **98**, 196405 (2007)
91. O. Visser, P. Aerts, D. Hegarty, W. Nieuwpoort, Chem. Phys. Lett. **134**, 34 (1987)

92. W. Liu, Mol. Phys. **108**, 1679 (2010)
93. A. Wolf, M. Reiher, B.A. Hess, J. Chem. Phys. **117**, 9215 (2002)
94. M. Douglas, N.M. Kroll, Ann. Phys. **82**, 89 (1974)
95. B.A. Hess, Phys. Rev. A **33**, 3742 (1986)
96. W. Liu, D. Peng, J. Chem. Phys. **125**, 044102 (2006)
97. F. Egidi, J.J. Goings, M.J. Frisch, X. Li, J. Chem. Theory Comput. **12**, 3711 (2016)
98. D. Peng, N. Middendorf, F. Weigend, M. Reiher, J. Chem. Phys. **138**, 184105 (2013)
99. W. Liu, Natl. Sci. Rev. **3**, 204 (2016)
100. M.A. Marques, M.J. Oliveira, T. Burnus, Comp. Phys. Comm. **183**, 2272 (2012)
101. S. Lehtola, C. Steigemann, M.J. Oliveira, M.A. Marques, SoftwareX **7**, 1 (2018)
102. C.A. Ullrich, Phys. Rev. B **72**, 073102 (2005)
103. F.G. Eich, S. Pittalis, G. Vignale, Phys. Rev. B **88**, 245102 (2013)
104. K. Goto, R.A. Geijn, ACM Trans. Math. Softw. **34**, 12 (2008)
105. Q. Wang, X. Zhang, Y. Zhang, Q. Yi, *AUGEM: automatically generate high performance dense linear algebra kernels on x86 CPUs*, in *Proceedings of the international conference on high performance computing, networking, storage and analysis* (ACM, 2013), p. 25
106. Z. Xianyi, W. Qian, Z. Yunquan, *Model-driven level 3 BLAS performance optimization on loongson 3A processor*, in 2012 *IEEE 18th international conference on parallel and distributed systems (ICPADS)* (IEEE, 2012), pp. 684–691
107. F.G. Van Zee, R.A. van de Geijn, ACM Trans. Math. Softw. **41**, 14 (2015)
108. Intel(r) math kernel library, 2016, 18.0. update 1 for linux
109. V. Lebedev, Sib. Math. J. **18**, 99 (1977)
110. S. Yamanaka, D. Yamaki, Y. Shigeta, H. Nagao, K. Yamaguchi, Int. J. Quant. Chem. **84**, 670 (2001)
111. J. Schimpl, H.M. Petrilli, P.E. Blöchl, J. Am. Chem. Soc. **125**, 15772 (2003)
112. S. Luo, I. Rivalta, V. Batista, D.G. Truhlar, J. Phys. Chem. Lett. **2**, 2629 (2011)
113. S. Luo, D.G. Truhlar, J. Chem. Theory Comput. **9**, 5349 (2013)
114. J.J. Goings, F. Ding, M.J. Frisch, X. Li, J. Chem. Phys. **142**, 154109 (2015)
115. X. Li, E.F. Valeev, D. Williams-Young, A. Petrone, J. Goings, J. Kasper, F. Ding, H. Liu, S. Sun, P. Lestrange, Chronus quantum, beta 2 version, 2017, http://www.chronusquantum.org
116. A.D. Becke, J. Chem. Phys. **98**, 5648 (1993)
117. C. Lee, W. Yang, R.G. Parr, Phys. Rev. B **37**, 785 (1988)
118. B. Miehlich, A. Savin, H. Stoll, H. Preuss, Chem. Phys. Lett. **157**, 200 (1989)
119. X. Li, S.M. Smith, A.N. Markevitch, D.A. Romanov, R.J. Levis, H.B. Schlegel, Phys. Chem. Chem. Phys. **7**, 233 (2005)
120. F. Ding, J.J. Goings, M.J. Frisch, X. Li, J. Chem. Phys. **141**, 214111 (2014)
121. L. Konecny, M. Kadek, S. Komorovsky, O.L. Malkina, K. Ruud, M. Repisky, J. Chem. Theory Comput. **12**, 5823 (2016)
122. J.J. Goings, P.J. Lestrange, X. Li, WIREs Comput. Mol. Sci. **8**, e1341 (2018)
123. R. Beck, A. Petrone, J.M. Kasper, M.J. Crane, P.J. Pauzauskie, X. Li, J. Phys. Chem. C **14**, 1998 (2018)
124. J.C. Slater, Phys. Rev. **81**, 385 (1951)
125. S.H. Vosko, L. Wilk, M. Nusair, Can. J. Phys. **58**, 1200 (1980)
126. T. Noro, M. Sekiya, T. Koga, Theor. Chem. Acc. **131**, 1124 (2012)
127. A. Bruner, D. LaMaster, K. Lopata, J. Chem. Theory Comput. **12**, 3741 (2016)
128. M. Repisky, L. Konecny, M. Kadek, S. Komorovsky, O.L. Malkin, V.G. Malkin, K. Ruud, J. Chem. Theory Comput. **11**, 980 (2015)
129. Z. Li, B. Suo, Y. Zhang, Y. Xiao, W. Liu, Mol. Phys. **111**, 3741 (2013)
130. F. Wang, T. Ziegler, E. van Lenthe, S. van Gisbergen, E. Jan Baerends, J. Chem. Phys. **122**, 204103 (2005)
131. M. Kühn, F. Weigend, J. Chem. Theory Comput. **9**, 5341 (2013)
132. A. Nakata, T. Tsuneda, K. Hirao, J. Chem. Phys. **135**, 224106 (2011)